

Energetic regimes and growth mechanisms of pulsed laser deposited Pd clusters on Au(111) investigated by *in situ* scanning tunneling microscopy

C. S. Casari,^{1,2,*} S. Foglio,¹ M. Passoni,¹ F. Siviero,^{1,†} C. E. Bottani,^{1,2} and A. Li Bassi^{1,2}

¹*Dipartimento di Energia and NEMAS, Center for NanoEngineered Materials and Surfaces, Politecnico di Milano, via Ponzio 34/3, I-20133 Milano, Italy*

²*Center for Nano Science and Technology @PoliMi, Istituto Italiano di Tecnologia, Via Pascoli 70/3 I-20133 Milano, Italy*

(Received 28 July 2011; published 28 October 2011)

Pulsed laser deposition (PLD) and *in situ* scanning tunneling microscopy (STM) have been employed here to investigate different deposition regimes for the synthesis of Pd nanoislands on Au(111). Atom-by-atom deposition at high kinetic energy or cluster deposition at different kinetic energies are allowed by PLD depending on experimental conditions. At variance with evaporation, which results in Pd island nucleation at the elbows of the $22 \times \sqrt{3}$ herringbone reconstruction of Au(111), PLD in vacuum leads to random island nucleation with a profound modification of surface reconstruction. In addition, deposition of preformed Pd clusters can be obtained by ablating in the presence of a background gas, and the deposits turn out to be strongly affected by both the energetic regime and by the complex anisotropic structure of the substrate surface. Low energy deposition allowed us to deposit ultrafine clusters (<2 nm), which aggregate in islands at preferential sites of the Au(111) reconstructed surface. Comparison with atom-by-atom deposition (i.e. evaporation), in which island size is strongly related with coverage and leads to lifting of the reconstruction at a coverage well below 40%, shows that low energy deposition by PLD results in a cluster arrangement nicely following the underlying surface reconstruction, in parallel rows at 40% coverage and in a zig-zag fashion for coverages up to 70%. Analysis of this deposition regime reveals that it follows a deposition diffusion aggregation (DDA) model of growth with some peculiar characteristics related to the supporting Au(111) surface reconstruction.

DOI: [10.1103/PhysRevB.84.155441](https://doi.org/10.1103/PhysRevB.84.155441)

PACS number(s): 68.55.A–, 68.37.Ef, 81.15.Fg

I. INTRODUCTION

Deposition of preformed clusters at surfaces involves a number of basic physical processes affecting the shape and the arrangement of clusters on a surface and the mechanisms of film growth.¹ Such processes, related to the synthesis of nanostructured surfaces, are of potential interest in a number of relevant applications ranging from magnetism to optics and catalysis.² Isolated metal clusters at surfaces are commonly used as catalyzing agents in the growth of nanostructures, such as nanowires and nanotubes,^{3,4} and are of great interest as model systems for heterogenous catalysis studies.⁵ For such applications, the control of cluster size and shape and of their position on the surface is of particular importance to design the final properties of the system. At variance with clusters grown by atom deposition, which exploits basic surface-atom processes for islands nucleation (e.g. Volmer–Weber growth), the deposition of clusters formed in the gas phase has the advantage of separating the process of cluster nucleation from the interaction with and dynamics on the surface. For cluster deposition, surface processes, such as diffusion, pinning, and aggregation, usually display complex features, becoming strongly dependent on their size and shape. In addition, new physical phenomena, such as cluster disruption, implantation, and surface damage, or alternatively, cluster soft landing and assembling, can be observed depending on the deposition kinetic energy.^{6–8}

Among physical vapor deposition methods, pulsed laser deposition (PLD) offers a peculiar versatility and some advantages. It has been shown that PLD under vacuum conditions, even at room temperature, results in a higher island nucleation density with respect to molecular beam epitaxy (MBE), thus allowing atom-by-atom deposition of films with a controlled

layer-by-layer morphology.^{9–12} Moreover, it is known that laser ablation in the presence of an inert background gas results in a spatial confinement of the expanding plasma favoring cluster formation due to increased collision rate with the surrounding gas molecules^{13–15} and thus allowing deposition of preformed clusters and growth of cluster-assembled materials.¹⁶

In this framework, the comprehension of the parameters affecting plasma expansion dynamics and their role in regulating the deposition process is fundamental for the synthesis and deposition of clusters and for the growth of cluster-assembled films with tailored properties. In the case of tungsten clusters, we already demonstrated that, by controlling background gas pressure and target-to-substrate distance, it is possible to vary the aggregation and energetic regime of ablated particles, which results in a control of cluster size and shape starting from isolated clusters supported on surfaces to the first stages of film formation and up to the growth of a nanostructured film.^{17–19}

We here exploit such capability for the preparation of metal (Pd) clusters supported on surfaces which represent systems of interest for heterogeneous catalysis applications. Among the others, the Pd-Au system is interesting for its role in different catalytic processes, as an Au-Pd surface alloy^{20,21} and in the form of Pd and bimetallic Pd-Au clusters.²² In addition, the Au(111) $22 \times \sqrt{3}$ surface, displaying the so-called herringbone reconstruction, represents an intriguing substrate: its characteristic arrangement due to a periodic change in domain orientation provides an ordered array of preferred nucleation sites. Au(111) is in fact an ideal template for the growth of self-organized ordered nanostructures since it is well known that some evaporated metal atoms (i.e. Pd, Fe, Co, Ni, Ti, Mo, and Pt) nucleate in nanosized islands ordered along specific sites (i.e. elbows) of the reconstructed

surface.^{23–30} Although the deposition of Pd atoms on Au(111) has been investigated by several authors, both experimentally and theoretically,^{24,25,31} the behavior of preformed Pd clusters deposited on Au(111) is still a completely open issue.

We report on an *in situ* scanning tunneling microscopy (STM) investigation of Pd clusters produced by PLD in the presence of a background inert gas and deposited on Au(111). Pd cluster deposition has been accomplished in an inert background atmosphere by varying the target-to-substrate distance to explore different energy deposition regimes. The effect the PLD parameters have on cluster deposition and diffusion on the surface has been investigated observing the resulting nanoscale morphology by STM and has been compared with evaporation in vacuum. The model of growth of low energy cluster deposition by PLD has been analyzed.

II. EXPERIMENTAL DETAILS

A commercial Au(111) evaporated on mica substrate was cleaned in a ultra high vacuum (UHV) preparation chamber (base pressure $<10^{-8}$ Pa) by 1 keV Ar⁺ sputtering for 15 min with the sample temperature maintained at 800 K for at least 20 min before cooling down to room temperature. An STM characterization of the clean as-prepared Au(111) surface was performed in order to check for contaminations and verify the presence of the Au(111) $22 \times \sqrt{3}$ herringbone reconstruction. UHV STM and preparation chambers are connected to the deposition chamber (base pressure $<10^{-6}$ Pa) allowing *in situ* characterization of PLD deposits.

Pulsed laser deposition of Pd at room temperature was accomplished exploiting a KrF excimer laser ($\lambda = 248$ nm, pulse duration = 10–15 ns), focused on a high-purity Pd (99.99%) polycrystalline target. The laser energy density (fluence) was set at 1.2 J/cm² at the target surface, and the number of laser pulses was chosen before each deposition according to the deposition rate (determined by a quartz crystal microbalance) in order to obtain the desired coverage. Argon (99.9999%) was used as the background gas at a pressure of 40 Pa. The target-to-substrate distance d_{t-s} was varied in the 30–80-mm range. At every chosen deposition pressure, the time integrated visible plume length l_p was measured from pictures of the plume taken with a digital camera. Evaporation of Pd was performed with an e-beam UHV evaporator equipped with a high-purity Pd (99.99%) rod and an ion flux monitor to control the evaporation rate.

After deposition, the sample was transferred to the STM chamber (base pressure $<10^{-8}$ Pa) equipped with an Omicron UHV VT-SPM. Scanning tunneling microscopy images were acquired at room temperature in constant-current mode with a bias in the ± 1 -V range and a tunneling current in the 0.1–2-nA range, using homemade electrochemical etched W tips.

Care was taken to reduce as much as possible contaminations during deposition; however, we cannot exclude the presence of contaminations. On the basis of the obtained results, we can reasonably exclude that contaminations play an important role in determining the morphology and growth of Pd clusters on Au(111).

III. RESULTS AND DISCUSSION

Atom-by-atom deposition regime was accomplished by ablation in vacuum, while cluster deposition was obtained by ablation in the presence of an Ar background gas atmosphere. In particular, when ablating in gas and in order to tune the cluster deposition process, we obtained different deposition regimes by changing the nondimensional parameter L defined as the ratio of the target-to-substrate distance d_{t-s} to the time integrated visible plume length l_p ($L = d_{t-s}/l_p$), as we already proposed in a previous work.³² In fact, in the presence of a background gas, a shock front can form during plume expansion, whose maximum distance defines the plume length l_p . We have already demonstrated that plume length l_p can be tuned by controlling the background gas pressure (at fixed laser fluence) and that the substrate position (d_{t-s}) with respect to the plume length can affect size and energy of deposited species and consequently the film growth mode and the film morphological and structural properties.^{17–19,32} In a simplified picture, we showed that when the substrate is out of plume ($L > 1$), ablated species can diffuse in the background gas beyond the maximum expansion length of the plume shock front (i.e. stopping distance), thus undergoing a significant reduction of their kinetic energy before impinging on the substrate.³³ Conversely, when the substrate is in plume ($L < 1$) ablated species reach the substrate after a less effective interaction with the surrounding background gas and thus with a higher kinetic energy compared to out-of-plume depositions. Many experimental and theoretical works have been devoted to the measurement of the kinetic energy of ablated species in vacuum. Usually, kinetic energy varying from several tens to hundreds of eV are considered when dealing with ablation in vacuum, and the reported values are strongly influenced by laser fluence and by the ablated material. For instance, Pt ions of about 100 eV have been reported when ablating a Pt target with a laser fluence of about 1.5–2 J/cm².¹¹ Irissou *et al.* systematically investigated the kinetic energy variation as a function of target-to-substrate distance and pressure for ablation of Au in the presence of different gases.³⁴ By inspecting the data they reported (i.e. Fig. 4 of Ref. 34) for ablation in Ar and assuming a similar behavior of Pd and Au, we expect that in our experimental conditions (fixed pressure 40 Pa Ar and varying d_{t-s} in the 30–80-mm range) kinetic energies between 0.1 and 1 eV/atom are obtained when $d_{t-s} = 30$ mm ($L = 0.7$), about 0.1 eV/atom when $d_{t-s} = 60$ mm ($L = 1.3$) and energies well below 0.1 eV/atom when $d_{t-s} = 80$ mm ($L = 1.7$).

A. Atom-by-atom deposition

Atom-by-atom Pd deposition on Au(111) by PLD is accomplished by ablating in vacuum, and the resulting morphology is shown in Fig. 1 where STM images of PLD and evaporated Pd deposits at similar coverages (about 10%) are compared. Pd evaporation on the Au(111) $22 \times \sqrt{3}$ herringbone reconstruction leads to the well-known preferential island growth at the two types of elbows (called pinched and bulged) formed by 120° angle rotation of the parallel ridges, as already reported in detail in previous works.^{24,31} The cluster size distribution for evaporation at a coverage of about 10% ranges

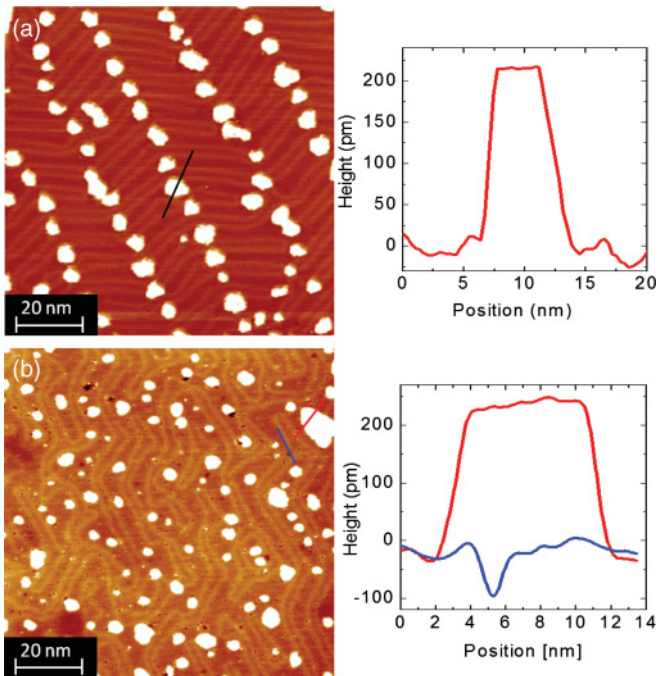


FIG. 1. (Color online) (a) STM image of Pd evaporation in vacuum (coverage is about 12%) and height profile of an island. Imaging conditions are: $I = 0.086$ nA; $V = -0.45$ V. (b) STM image of Pd deposited on Au(111) by PLD in vacuum condition (10^{-5} Pa, $d_{t-s} = 80$ mm, 25 laser pulses, coverage 10%) and height profiles showing a Pd island and a hole. Imaging conditions are: $I = 0.067$ nA; $V = +0.81$ V.

from 3 to 8 nm with a mean size of 5.1 nm. Conversely, PLD in vacuum leads to a substantially different deposition mechanism. Pd islands showing a size distribution ranging from 2 to 10 nm (4.2 nm mean size) are randomly arranged on the surface, and the underlying Au(111) reconstruction lost its characteristic periodic pattern, showing randomly oriented ridges surrounding island borders without crossing or passing below them. The topography profile of a Pd island deposited by PLD (see Fig. 1(b)) shows one monolayer (ML) high and flat islands quite similar to evaporated Pd islands and typical of atom-by-atom deposition. Despite this similarity, the random island distribution is a peculiar effect of the PLD process in vacuum. Moreover, the whole surface is densely dotted with small holes [70–90-pm depth, see Fig. 1(b)] randomly distributed on the surface. To interpret these findings, we observe that ablation in vacuum leads to a large fraction of atoms impinging the substrate after a nearly collisionless flight from the target with a kinetic energy that can be as high as 100 eV.¹¹ In such a deposition regime, implantation, surface damage and even sputtering phenomena are expected since the cohesive energy of the surface (3.81 eV/atom in the case of bulk Au³⁵) is substantially lower than the energy of the incoming species. In this case, implanted atoms and surface defects can act as nucleation centers, thus hindering the role of elbows as preferential sites. We also observe the disordering of the herringbone reconstruction, which has been already observed in the literature for high coverage of evaporated Pd^{24,31} and Co³⁶ and explained as a relaxation effect of the Au(111) topmost layer, stressed by the island growth. In our

case, also the effect of vacancy formation by sputtered atoms must be considered, which may lead to an unbalance in the complex Au(111) reconstruction that rearranges to minimize the surface stress.

B. Cluster deposition at different energy regimes

We performed Pd depositions in a background gas by varying the L value in the 0.7–1.7 range as shown in the STM images reported in Fig. 2. The L value was varied by changing the target-to-substrate distance while keeping constant all the other parameters (i.e. 40 Pa Ar pressure and laser fluence). Deposition at $L = 0.7$ does not substantially affect the herringbone reconstruction, and Pd islands are present both at the elbows and in between discommensuration lines. In addition, wide dark regions (size comparable to islands and depth of about 30 pm) are clearly visible in correspondence of all elbows, whether decorated with an island or not. Such dark regions are considerably larger and shallower than holes observed for PLD in vacuum; dark regions were observed nearby elbows also for evaporated Pd atoms at very low coverages and were attributed to Pd substitution sites as the basic mechanism for further island formation.³¹ In the case of evaporation, we previously investigated this effect showing that those regions are about 30 pm (apparent height in constant-current images) below the surface level, and atomically resolved images seemed to suggest the presence of substituted Pd atoms embedded in the Au(111) surface layers.²⁴ Recently, similar features observed by Baber *et al.* were assigned to the presence of subsurface substituted atoms.³⁷ In addition, the mechanisms for preferential nucleation and the role of embedded Pd atoms in Au surface layer have been addressed theoretically by several authors.^{25,38–40} The reasons for such contrast differences between Pd and Au atoms were not completely explained. The interpretation of dark regions as Pd species embedded in the Au surface is further supported by an analysis of the electronic contrast by differential conductivity (dI/dV) maps as discussed in Sec. III.D.

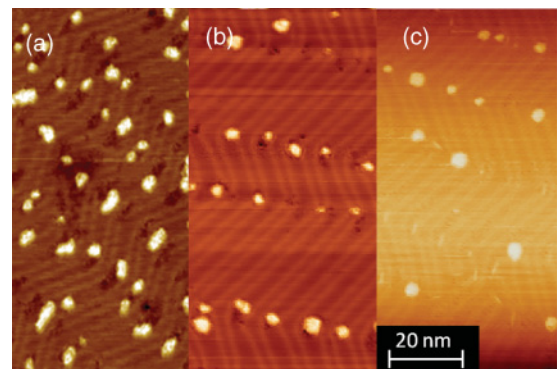


FIG. 2. (Color online) STM images of Pd clusters deposited on Au(111) by PLD at 40 Pa Ar: (a) deposition at $L = 0.7$ ($d_{t-s} = 30$ mm, 20 laser pulses, coverage $\theta = 7.3\%$), imaging conditions are: $I = 0.055$ nA; $V = -1.26$ V; (b) deposition at $L = 1.3$ ($d_{t-s} = 45$ mm, 5 laser pulses, coverage $\theta = 3\%$), imaging conditions are: $I = 0.2$ nA; $V = -0.47$ V; (c) deposition at $L = 1.7$ ($d_{t-s} = 80$ mm, 15 laser pulses) coverage $\theta = 2.1\%$, imaging conditions are: $I = 0.436$ nA; $V = -0.84$ V.

In PLD, we found that more and larger dark regions are present with respect to evaporation. This occurrence may be related with the higher kinetic energy of impinging species which may lead to a larger fraction of substituted atoms or resputtering of already formed islands. In fact, for a deposition at $L = 0.7$ [see image reported in Fig. 2(a)], the island coverage of the surface, estimated from STM images, is about 7%, although a higher value (about 20%) was estimated by measuring the deposition rate with a quartz microbalance exactly in the same conditions. Although the origin of dark regions in the STM images is due to an electronic contrast, and the number of Pd atoms embedded in or below the surface cannot be directly measured by the measured area, we noticed that the coverage rises up to about $\theta = 20\%$ if dark regions are included in the evaluation of Pd coverage from STM images, suggesting that, at this stage of growth, embedded Pd atoms in the Au(111) surface layers are not negligible. We underline that the presence of a background gas slows down the more energetic species, and resputtering effects can be considered increasingly reduced as the L value is increased. In fact, we observe a better agreement between coverage measured by quartz microbalance and the Au(111) coverage observed by STM images together with a decrease of dark regions when moving from $L = 0.7$ to 1.7. For instance, at $L = 1.3$, an island coverage of $\theta = 12.5\%$ increases only to 14% when including dark regions.

Deposition at $L = 1.3$ [see Fig. 2(b), coverage $\theta = 3\%$] is characterized by islands mainly present at the elbows and sometimes along the ridges. Dark regions are less than in the case $L = 0.7$ and are mainly found at elbow sites. At $L = 1.7$, the surface appears covered [see Fig. 2(c), coverage $\theta = 2.1\%$] by islands located at the elbows, while dark regions are negligible, even at these lower coverages, with respect to deposition at $L = 0.7$. We underline that, in all these conditions (i.e. $0.7 < L < 1.7$) and for low coverages, the Au(111) herringbone reconstruction is preserved, thus indicating a softer deposition regime with respect to PLD in vacuum.

We have shown that the substrate position with respect to the maximum distance reached by the plume shock front (i.e. the L parameter) allows variation of the cluster deposition regimes. For a fixed pressure, controlling the L value (i.e. changing the target-to-substrate distance) corresponds to changing the velocity of impinging species, as shown, for instance, by Riabibina *et al.* in the case of Pt ablated in the presence of He.⁴¹ In general, the L value can be used as a rough indicator of the slowing effect of the background gas on the ablated species, and it sets a relation between two fundamental parameters in PLD, such as background gas pressure and target-to-substrate distance. In the case of Pd on Au(111), we observed that changing the pressure from 40 to 10 Pa at a fixed L value of 1.3 leads to very similar results (not shown). This outcome can be somehow generalized also for other systems. For instance, for W clusters deposited on Au(111), we found a similar behavior in terms of surface damage for in-plume deposition and cluster soft landing for out-of-plume deposition, while no preferential order of W clusters at elbows was observed.¹⁸ Of course, the energy deposition regime profoundly affects the growth of a film, and we have already shown that film morphology and structure can be tuned from compact/columnar to cluster-assembled (from

hierarchical tree-like to open porous sponge-like) for a number of metal oxides (i.e. WO_3 , TiO_2 , Ag_4O_4 , and Al_2O_3).^{19,32,42-44} Other aspects, which are beyond the scope of this paper, need to be investigated, such as the mechanisms of cluster nucleation in the plume and the effect that the deposition conditions may have in determining the size of deposited species.

C. Low energy cluster deposition

In order to investigate the deposition mechanisms leading to supported clusters and eventually to cluster-assembled materials retaining memory of the nanosized building blocks, we now focus on cluster deposition at $L = 1.3$, allowing soft landing of clusters on the substrate. For low coverage ($\theta = 1\%$, see Fig. 3), a few Pd islands of about 3.5 nm mean size are present together with ultrafine clusters of about 0.5 nm average diameter, which are collected mainly in correspondence of the step edge, as evidenced by the bimodal size distribution. Since the ablated species are deposited at random positions on the surface, we suppose that the small clusters observed on step edges nucleated in the plasma plume before impinging the substrate. Concerning the larger Pd islands, we observe two different kinds, as shown in Fig. 4. One type of island is characterized by a flat, regularly shaped central part, about 2 nm wide and with the height of a single Pd monolayer (0.2 nm). About 70% of observed islands, at this early stage of growth, show the same flat structure at their center, suggesting they are composed by atoms diffusing on the surface together with clusters.^{13,45,46} Such islands appear decorated by small clusters with a mean size of about 0.5 nm. Other kinds of islands are constituted by an assembly of clusters of the same size (about 0.5 nm). Those islands are approximately of the same size as the flat ones but with a slightly lower height (about 0.15 nm instead of 0.2 nm) and with the presence of depressions which may reveal a partial inclusion in the substrate.

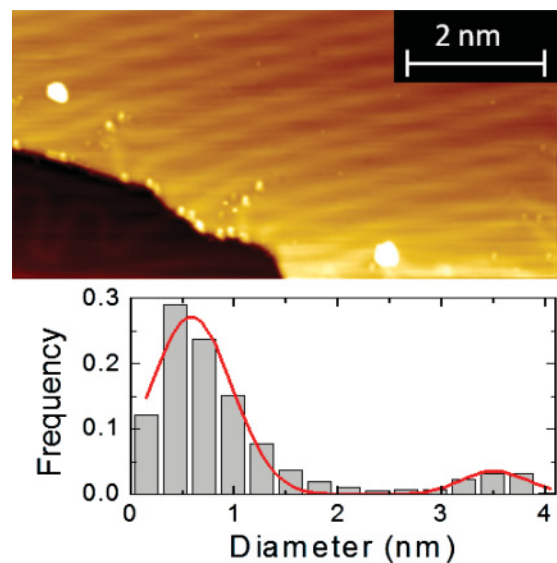


FIG. 3. (Color online) STM image of a deposition at $L = 1.3$ ($d_{t-s} = 45$ mm, 3 laser pulses) at low coverage ($\theta < 1\%$) and size distribution of Pd deposits. Imaging conditions are: $I = 0.118$ nA; $V = -0.53$ V.

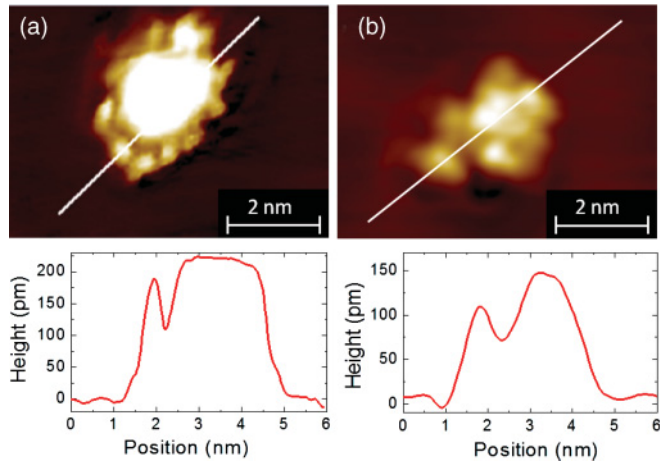


FIG. 4. (Color online) STM image and height profile of two types of Pd clusters observed for deposition at $L = 1.3$ at a coverage $\theta < 1\%$ (3 laser pulses): (a) monolayer island decorated by clusters (imaging conditions are: $I = 0.224$ nA; $V = 0.51$ V) and (b) island made by aggregation of ultrafine (0.5 nm) clusters (imaging conditions are: $I = 0.126$ nA; $V = 1.7$ V).

Scanning tunneling microscopy images of depositions at $L = 1.3$ with increasing coverage from 2.5% to 72% are shown in Fig. 5 and are compared with evaporation in vacuum. At a Pd coverage of $\theta = 2.5\%$, islands nucleate nearby elbows of the herringbone reconstruction; the fraction of flat islands is substantially reduced to the advantage of the cluster-assembled ones. Evaporation at the same coverage (2.9%) shows quite the same morphology and arrangement of Pd islands. At a coverage of $\theta = 12.5\%$, islands still nucleate mainly in correspondence of the elbows. Even if the amount of deposited material is increased, the mean island size is about 4 nm, close

to that observed at lower coverage while the distribution is broader due to a small increase of the number of species larger than 6 nm. At this coverage, 95% of elbows are filled with an island, meaning that a large part of Pd deposited on the surface was addressed to the nucleation of a new island on a free elbow. For comparison, we observe that in the case of evaporation, at a similar coverage (14%), all preferential nucleation sites (i.e. elbows) are occupied by a Pd island (i.e. elbows have been saturated). Going back to the PLD case, the saturation point for which all the elbows are occupied is reached at a coverage of about 40%, and the surface is characterized by clusters often grouped in two or three and arranged in parallel rows separated by empty regions corresponding to the straight ridges of the Au(111) reconstruction. Once all the elbows are occupied, the incoming Pd species prefer to occupy the interstices between elbows and to contribute to the growth of an existing island, rather than nucleate a new island in an unfavorable zone. This is clearly observable when evaporating at a coverage of 38%: islands grow further and coalesce; the ordered arrangement is lost, even with a disordering of the underlying herringbone reconstruction. Such behavior is peculiar of Pd on Au(111) since for instance Morgenstern *et al.* reported Co deposition showing ordered islands without coalescence up to a coverage of 70% (but with islands up to 4 ML high).⁴⁷ Different from evaporation, we observed that at low energy regimes, PLD of Pd clusters does not substantially modify the Au(111) reconstruction, regardless of the amount of material deposited. Thanks to this, deposition at 72% coverage is characterized by Pd islands expanding in the direction of the straight ridges, giving rise to a nearly complete film with a fascinating zig-zag morphology that keeps the track of the underneath surface reconstruction. Such observations mark the differences between atom-by-atom evaporation and low energy cluster deposition.

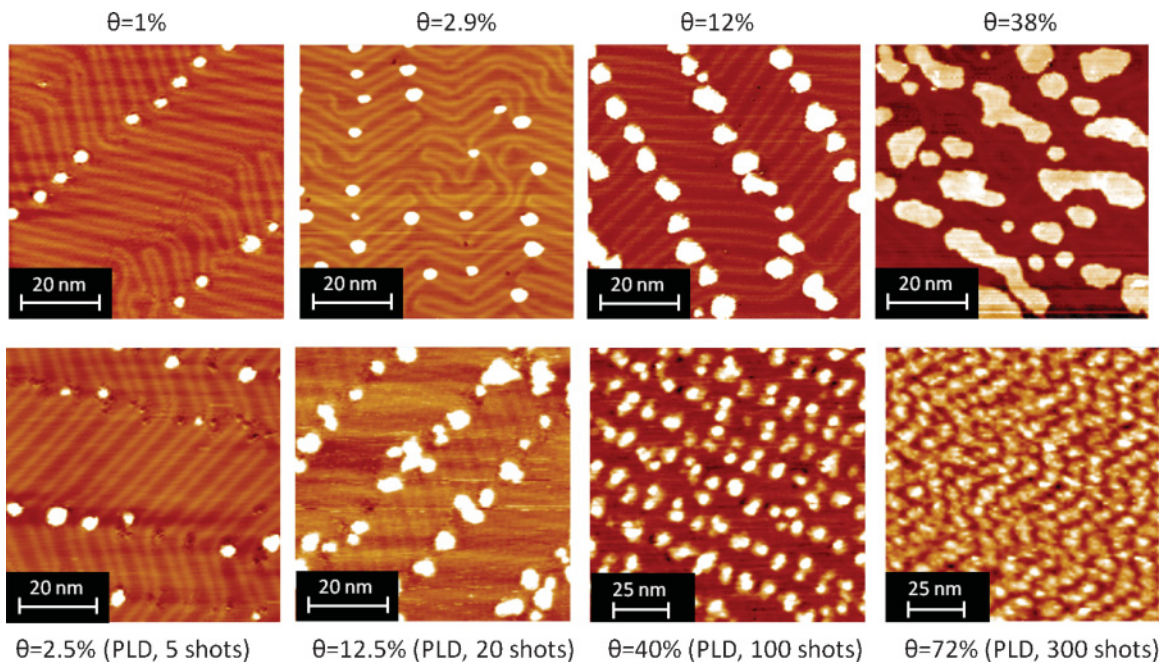


FIG. 5. (Color online) Comparison of STM images at increasing coverages between Pd evaporation in vacuum (top row) and Pd clusters deposited by PLD at $L = 1.3$ (40 Pa Ar, $d_{t-s} = 45$ mm) (bottom row). All the images are reported with the same z range (500 pm) and with the same color contrast.

Cluster deposition allows increase of the coverage without affecting the island size and without removing the herringbone reconstruction. Clusters produced in the plume, presumably the fine clusters about 0.5 nm in size, have sufficient mobility on the surface to fill the elbows and to form cluster-assembled islands, while at the same time they can occupy other sites when all the elbows are occupied. This occurrence and the reduced coalescence between clusters finally prevent island growth further and lift of the surface reconstruction.

D. Cluster deposition and growth model

With the aim of investigating the growth model in the low energy cluster deposition regime, we studied the evolution of Pd coverage as a function of the number of laser shots for different depositions performed at 40 Pa with $L = 1.3$. As discussed below, we observe a nonlinear behavior, which implies the existence of a diffusion barrier at the edge of the islands that prevents a cluster from falling down when it is deposited directly on an already formed island. Such behavior was discussed in detail by Bardotti *et al.*,⁴⁸ describing the deposition diffusion aggregation (DDA) model in the growth of fractal islands observed in low energy cluster beam deposition of Sb and Au clusters on highly oriented pyrolytic graphite (HOPG). The DDA model assumes cluster diffusion on the surface subsequent to a random deposition, a sticking coefficient between cluster and surface equal to one, and irreversible cluster-cluster and cluster-islands sticking. Additional assumptions neglecting cluster diffusion along island edges and cluster coalescence were adopted by Bardotti *et al.* to account for the observation of Sb and Au ramified islands on HOPG. We observed the formation of similar ramified islands for PLD deposition of W clusters on HOPG,¹⁷ while we do not observe any ramified islands for Pd on Au(111), since its surface reconstruction is a more complex system which involves preferential diffusion directions for Pd clusters and nucleation centers for Pd island formation. In such a case, we cannot exclude cluster diffusion along island edges and a partial cluster coalescence, even though we can still recognize the cluster structure forming the islands.

Here, to perform a detailed analysis of the growth mode in the low energy deposition regime ($L = 1.3$, 40 Pa Ar), we have to correctly measure the Pd coverage as a function of the number of laser shots. In order to gain a better insight on the presence of Pd on the Au(111) surface and in particular in the dark regions, we acquired scanning tunneling spectroscopy (STS) curves and dI/dV differential conductivity maps. In Fig. 6, a constant current STM image and a dI/dV map are compared, and in both images, Pd clusters appear bright and are clearly distinguished from the Au surface. Depressions (i.e. dark regions) in topography images exhibit, in the dI/dV map, a similar contrast as the islands, suggesting comparable electronic properties (i.e. local density of states LDOS at -1 eV). Analogous results were obtained comparing the contrast of Pd clusters and depressions in dI/dV maps taken at -0.3 and 0.5 V (not shown). Here, dI/dV curves acquired on specific sites, namely the Au(111) surface, dark regions, and Pd clusters, point out some differences in the LDOS of the three sites. Such differences are even more evident after proper normalization of the dI/dV curves in order to exclude

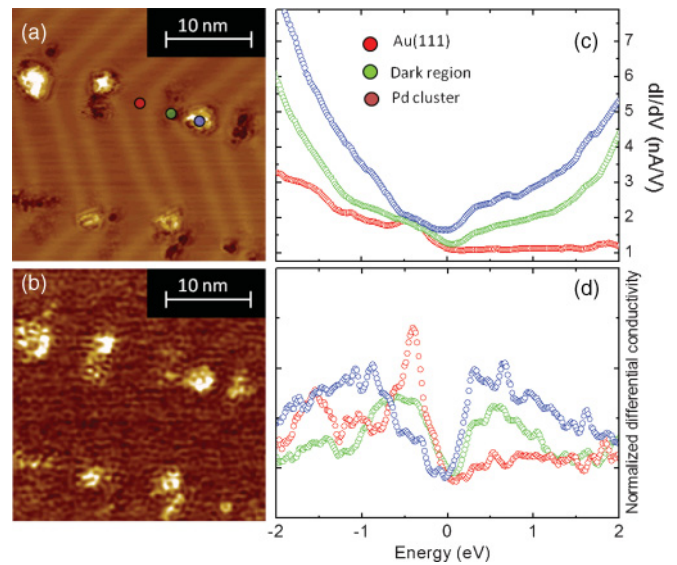


FIG. 6. (Color online) (a) STM images of Pd clusters deposited on Au(111) at $L = 1.3$ and about 2.5% coverage (40 Pa Ar, $d_{t-s} = 45$ mm, 5 laser shots). Depressions are clearly visible on empty elbows and nearby clusters. (b) Differential conductivity map (set points: $V = -0.9$ V, $I = 0.4$ nA) of the same area shown in (a). (c) dI/dV spectra of different sites (acquired at constant height for $V = 1$ V, $I = 1$ nA) corresponding to markers indicated in (a). (d) dI/dV spectra normalized with respect to the transmission coefficient (see text).

the contribution of the transmission coefficient by using the procedure we presented in a previous paper.⁴⁹ On Au(111), a peak at -0.4 V is clearly visible, corresponding to the Shockley state⁵⁰ completely missing in the curve taken on a Pd cluster. On the contrary, the spectrum acquired on a dark region exhibits a small feature at the same bias of the Au(111) Shockley state, showing an intermediate behavior between Au and Pd. The observation of a decreasing Au Shockley state when moving from the bare Au surface to regions with the presence of Pd atoms has some similarities with what has been observed on Au(111) by photoelectron spectroscopy in the valence band at increasing Pd coverage up to one monolayer.⁵¹ Even though we cannot consider STS data as an unequivocal fingerprint of each element, they are a first indication of a common chemical nature of Pd clusters and dark regions. Our STS analysis focused on clusters with diameter ranging from 3 to 5 nm, and no appreciable size dependence was found in the conductance curves, which is expected to change for cluster diameters lower than 2 nm.^{52,53}

Once the presence of Pd atoms in the dark regions has been evidenced, the Pd surface coverage was estimated, including the dark areas, and the plot is characterized by a decreasing slope with increasing number of laser shots, as shown in Fig. 6. Due to the lack of knowledge about the atomic structure of both clusters and dark regions, we here assumed the same density of Pd atoms in clusters and in dark regions, even though it is likely to expect a lower density in dark regions with respect to clusters. We fitted the experimental points according to the following formula for the evolution of the coverage θ :

$$\theta = 1 - \exp \left[- \left(\frac{\pi D_m^2}{4} \right) R N_p \right],$$

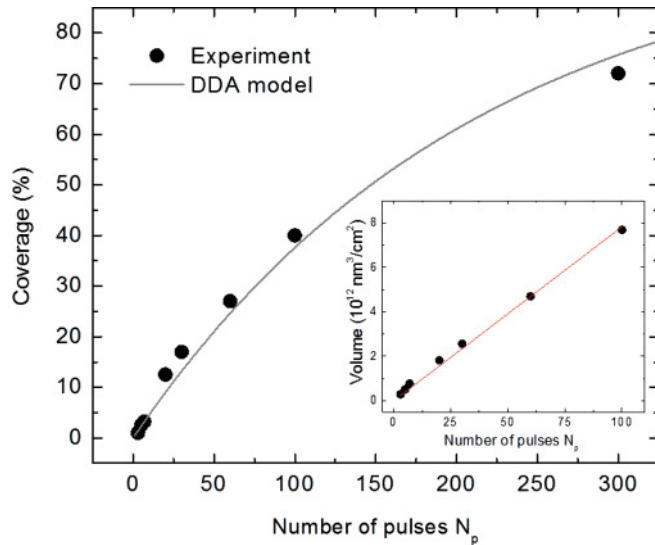


FIG. 7. (Color online) Plot of the surface Pd coverage as a function of laser pulses for depositions at $L = 1.3$. Experimental data (dots) are compared with theoretical DDA model (line). Deposited volume as a function of laser pulses used to calibrate the deposition rate is shown in the inset.

where D_m is the average diameter of clusters. We here adapted a model used for evaporation⁴⁸ to a pulsed deposition regime by introducing N_p as the number of laser pulses and R as the deposition rate per pulse. Here, R was estimated by evaluating the slope of the linear fit of the volume of Pd deposited per unit surface (considering both the volume of protruding clusters and dark regions) as a function of laser pulses (Fig. 7 inset). The deposited volume per pulse and per unit surface is $V = 7.8 \times 10^{10} \text{ nm}^3/\text{cm}^2$ and by using $V_C = 0.033 \text{ nm}^3$ as the mean cluster volume (estimated from STM image analysis), R is obtained:

$$R = V/V_C = 2.4 \times 10^{12} \left[\frac{\text{cluster}}{\text{pulse cm}^2} \right].$$

We plotted the coverage as a function of laser pulses, as shown in Fig. 7, and we found a nice agreement between experimental data (circles) and the model (line)

when $D_m = 0.5 \text{ nm}$ is considered, in agreement with the average cluster size estimated by STM images (Fig. 3).

IV. CONCLUSIONS

We investigated, by means of *in situ* STM imaging at the nanometer scale, different deposition regimes achievable in a PLD process by ablation of a Pd target in different conditions. The PLD atom-by-atom growth of Pd islands turns out to be profoundly different from standard evaporation due to the very different kinetic energy of the deposited species. In fact, by ablating in vacuum (high energy regime), the disordering of the herringbone reconstruction accompanied by random island nucleation takes place instead of the ordered growth along elbows of the herringbone reconstruction expected for evaporation (low energy regime). In addition, we showed that, for deposition of preformed clusters by ablation in the presence of a gas, deposition energy can be tuned by a proper positioning of the substrate with respect to the maximum distance of the plume shock front.

Conditions for a low energy regime allow for cluster soft landing on the substrate, and the growth mechanisms follow a DDA model. Islands are located at preferential sites, as for evaporation, but with a strongly reduced growth of island size with increasing the coverage (whereas island size and surface coverage are intimately correlated in the case of Pd evaporation), and with a negligible effect on the Au(111) surface reconstruction for coverages up to 70%, which is not achievable by evaporation. Hence, by exploiting Au(111) reconstruction, which is not distorted up to high coverages, linear or zig-zag nanowire structures can be created without the need of templates, opening new possibilities to realize nanometric structures self-assembled on the herringbone reconstruction. This versatility is of potential interest in a wide variety of applications related to clusters supported on surfaces. In particular, for the Pd on Au system, the possibility to deposit ultrafine particles is considered a key element for the development of catalytic systems displaying high functionality with a low content of noble metal.

ACKNOWLEDGMENT

The authors would like to acknowledge Guido Fratesi for suggestions and useful discussion.

*carlo.casari@polimi.it

†Present address: SAES Getters-R&D Labs, viale Italia 77, 20020 Lainate (Italy).

¹P. Jensen, *Rev. Mod. Phys.* **71**, 1695 (1999).

²H.-J. Freund, *Surf. Sci.* **500**, 271 (2002).

³X. Wang, C. J. Summers, and Z. L. Wang, *Nano Lett.* **4**, 423 (2004).

⁴G. Bertoni, C. Cepek, F. Romanato, C. S. Casari, A. Li Bassi, C. E. Bottani, and M. Sancrotti, *Carbon* **42**, 440 (2004).

⁵N. Nilius, *Prog. Surf. Sci.* **67**, 99 (2001).

⁶H. Haberland, Z. Insepov, and M. Moseler, *Phys. Rev. B* **51**, 11061 (1995).

⁷K. Bromann, C. Félix, H. Brune, W. Harbich, R. Monot, J. Buttet, and K. Kern, *Science* **274**, 956 (1996).

⁸D. Donadio, L. Colombo, P. Milani, and G. Benedek, *Phys. Rev. Lett.* **83**, 776 (1999).

⁹H. Jenniches, M. Klaua, H. Hoche, and J. Kirschner, *Appl. Phys. Lett.* **69**, 3339 (1996).

¹⁰J. Shen, Zheng Gaib, and J. Kirschner, *Surf. Sci. Rep.* **52**, 163 (2004).

¹¹M. Schmid, C. Lenauer, A. Buchsbaum, F. Wimmer, G. Rauchbauer, P. Scheiber, G. Betz, and P. Varga, *Phys. Rev. Lett.* **103**, 076101 (2009).

¹²S. H. Phark, Y. Jun Chang, T. W. Noh, and J. S. Kim, *Phys. Rev. B* **80**, 035426 (2009).

¹³D. B. Geohegan, A. A. Poretzky, G. Duscher, and S. J. Pennycook, *Appl. Phys. Lett.* **72**, 2987 (1998).

- ¹⁴E. Irissou, B. Le Droff, M. Chaker, and D. Guay, *J. Appl. Phys.* **94**, 4796 (2003).
- ¹⁵A. V. Bulgakov and N. M. Bulgakova, *J. Phys. D: Appl. Phys.* **31**, 693 (1998).
- ¹⁶D. H. Lowndes, D. B. Geohegan, A. A. Poretzky, D. P. Norton, and C. M. Rouleau, *Science* **273**, 898 (1996).
- ¹⁷D. Cattaneo, S. Foglio, C. S. Casari, A. Li Bassi, M. Passoni, and C. E. Bottani, *Surf. Sci.* **601**, 1892 (2007).
- ¹⁸D. Cattaneo, N. Righetti, C. S. Casari, A. Li Bassi, and C. E. Bottani, *Appl. Surf. Sci.* **253**, 7917 (2007).
- ¹⁹F. Di Fonzo, A. Bailini, V. Russo, A. Baserga, D. Cattaneo, M. G. Beghi, P. M. Ossi, C. S. Casari, A. Li Bassi, and C. E. Bottani, *Catalysis Today* **116**, 69 (2006).
- ²⁰M. Chen, D. Kumar, C. W. Yi, and D. W. Goodman, *Science* **310**, 291 (2005).
- ²¹F. Maroun, F. Ozanam, O. M. Magnussen, and R. J. Behm, *Science* **293**, 1811 (2001).
- ²²D. I. Enache, J. K. Edwards, P. Landon, B. Solsona-Espriu, A. F. Carley, A. A. Herzing, M. Watanabe, C. J. Kiely, D. W. Knight, and G. J. Hutchings, *Science* **311**, 362 (2006).
- ²³D. D. Chambliss, R. J. Wilson, and S. Chiang, *Phys. Rev. Lett.* **66**, 1721 (1991).
- ²⁴C. S. Casari, S. Foglio, F. Siviero, A. Li Bassi, M. Passoni, and C. E. Bottani, *Phys. Rev. B* **79**, 195402 (2009).
- ²⁵H. Bulou and J. P. Bucher, *Phys. Rev. Lett.* **96**, 076102 (2006).
- ²⁶M. Ø. Pedersen, S. Helveg, A. Ruban, I. Stensgaard, E. Lægsgaard, and F. Besenbacher, *Surf. Sci.* **426**, 395 (1999).
- ²⁷J. A. Stroschio, D. T. Pierce, R. A. Dragoset, and P. N. First, *J. Vac. Sci. Technol. A* **10**, 1981 (1992).
- ²⁸B. Voigtlander, G. Meyer, and N. M. Arner, *Surf. Sci.* **255**, L529, (1991).
- ²⁹M. Biener, J. Biener, R. Schalek, and C. M. Friend, *Surf. Sci.* **594**, 221 (2005).
- ³⁰J. Biener, E. Farfan-Arribas, M. Biener, C. M. Friend, and R. J. Madix, *J. Chem. Phys.* **123**, 094705 (2005).
- ³¹A. W. Stephenson, C. J. Baddeley, M. S. Tikhov, and R. M. Lambert, *Surf. Sci.* **398**, 172 (1998).
- ³²A. Bailini, F. Di Fonzo, M. Fusi, C. S. Casari, A. Li Bassi, V. Russo, A. Baserga, and C. E. Bottani, *Appl. Surf. Sci.* **253**, 8130 (2007).
- ³³S. Amoroso, A. Sambri, M. Vitiello, and X. Wang, *Appl. Surf. Sci.* **252**, 4712 (2006).
- ³⁴E. Irissou, B. Le Droff, M. Chaker, M. Trudeau, and D. Guay, *J. Mater. Res.* **19**, 950 (2004).
- ³⁵C. Kittel, *Introduction to Solid State Physics*, 6th ed. (John Wiley and Sons, New York, 1986), p. 55.
- ³⁶J. Kibsgaard, K. Morgenstern, E. Lægsgaard, J. V. Lauritsen, and F. Besenbacher, *Phys. Rev. Lett.* **100**, 116104 (2008).
- ³⁷A. Baber, H. L. Tierney, and E. C. H. Sykes, *ACS Nano* **4**, 1637 (2010).
- ³⁸H. Bulou and C. Goyhenex, *Phys. Rev. B* **65**, 045407 (2002).
- ³⁹D. Yuan, X. Gong, and R. Wu, *Phys. Rev. B* **75**, 085428 (2007).
- ⁴⁰G. Fratesi, *J. Phys.: Condens. Matter* **23**, 015001 (2011).
- ⁴¹D. Riabinina, E. Irissou, B. Le Droff, M. Chaker, and D. Guay, *J. Appl. Phys.* **108**, 034322 (2010).
- ⁴²F. Di Fonzo, C. S. Casari, V. Russo, M. F. Brunella, A. Li Bassi, and C. E. Bottani, *Nanotechnology* **20**, 015604 (2009).
- ⁴³D. Dellasega, A. Facibeni, F. Di Fonzo, M. Bogana, A. Polissi, C. Conti, C. Ducati, C. S. Casari, A. Li Bassi, and C. E. Bottani, *Nanotechnology* **19**, 475602 (2008).
- ⁴⁴F. Di Fonzo, D. Tonini, A. Li Bassi, C. S. Casari, M. G. Beghi, C. E. Bottani, D. Gastaldi, P. Vena, and R. Contro, *Appl. Phys. A* **93**, 765 (2008).
- ⁴⁵M. S. Tillack, D. W. Blair, and S. S. Harilal, *Nanotechnology* **15**, 390 (2004).
- ⁴⁶Y. Franghiadakis, C. Fotakis, and P. Tzanetakis, *Appl. Phys. A* **68**, 391 (1999).
- ⁴⁷K. Morgenstern, J. Kibsgaard, J. V. Lauritsen, E. Lægsgaard, and F. Besenbacher, *Surf. Sci.* **601**, 1967 (2007).
- ⁴⁸L. Bardotti, P. Jensen, A. Hoareau, M. Treilleux, B. Cabaud, A. Perez, and F. Cadete Santos Aires, *Surf. Sci.* **367**, 276 (1996).
- ⁴⁹M. Passoni, F. Donati, A. Li Bassi, C. S. Casari, and C. E. Bottani, *Phys. Rev. B* **79**, 045404 (2009).
- ⁵⁰M. P. Everson and R. C. Jaklevic, *J. Vac. Sci. Technol. A* **8**, 3662 (1990).
- ⁵¹T. Eguchi, A. Kamoshida, M. Ono, M. Hamada, R. Shoda, T. Nishio, A. Harasawa, T. Okuda, T. Kinoshita, and Y. Hasegawa, *Phys. Rev. B* **74**, 073403 (2006).
- ⁵²C. P. Vinod, G. U. Kulkarni, and C. N. R. Rao, *Chem. Phys. Lett.* **289**, 329 (1998).
- ⁵³A. Bifone, L. Casalis, and R. Riva, *Phys. Rev. B* **51**, 11043 (1995).